Radiation Dosimetry of a ^{99m}Tc-Labeled IgM Murine Antibody to CD15 Antigens on Human Granulocytes

P. David Mozley, James B. Stubbs, Stefan H. Dresel, Eleathea D. Barraclough, Terry Smith, Mohan Patel, Cynthia Finkelman, Richard B. Sparks, Mathew L. Thakur, Ajit Mathur and Abass Alavi

University of Pennsylvania, Philadelphia; Thomas Jefferson University, Philadelphia, Pennsylvania; Internal Dosimetry Systems of Oak Ridge, Oak Ridge, Tennessee; and Palatin Technologies, Inc., Princeton, New Jersey

^{99m}Tc-labeled anti-stage specific embryonic antigen-1 (anti-SSEA-1) is an injectable IgM antibody derived from mice. It binds to CD15 antigens on some granulocytic subpopulations of human white blood cells in vivo after systemic administration. The purpose of this study was to measure biodistribution of ^{99m}Tc-labeled anti-SSEA-1 and perform radiation dosimetry in 10 healthy human volunteers. **Methods:** Transmission scans and whole-body images were acquired sequentially on a dual-head camera for 32 h after the intravenous administration of about 370 MBq (10.0 mCi) of the radiopharmaceutical. Renal excretion fractions were measured from 10 to 14 discrete urine specimens voided over 27.9 ± 2.0 h. Multiexponential functions were fit iteratively to the time-activity curves for 17 regions of interest using a nonlinear least squares regression algorithm. The curves were integrated numerically to yield source organ residence times. Gender-specific radiation doses were then estimated individually for each subject, using the MIRD technique, before any results were averaged. **Results:** Quantification showed that the kidneys excreted 39.5% ± 6.5% of the administered dose during the first 24 h after administration. Image analysis showed that 10%–14% of the radioactivity went to the spleen, while more than 40% went to the liver. Residence times were longest in the liver (3.37 h), followed by the bone marrow (1.09 h), kidneys (0.84 h) and the spleen (0.65 h). The dose-limiting organ in both men and women was the spleen, which received an average of 0.062 mGy/MBq (0.23 rad/mCi, range 0.08–0.30 rad/mCi), followed by the kidneys (0.051 mGy/MBq), liver (0.048 mGy/MBq) and urinary bladder (0.032 mGy/MBq). The effective dose equivalent was 0.018 mSv/MBq (0.068 rem/mCi). **Conclusion:** The findings suggest that the radiation dosimetry profile for this new infection imaging agent is highly favorable.

Key Words: ^{99m}Tc; anti-stage specific embryonic antigen-1 antibody; infection; radionuclide

J Nucl Med 1999; 40:625–630

Infections remain the leading cause of death and disability in the world (*1*). Several radiotracers can be used to localize abscesses and phlegmons when structural imaging techniques fail (*2–8*). Although effective, these procedures are less than ideal (*9*). Among the problems are the relatively high radiation doses associated with most clinically available imaging agents (*10*). This limits the amount of radioactivity that can be administered and, as a consequence, reduces image quality and decreases diagnostic effectiveness.

The radiation dosimetry associated with ^{99m}Tc is much more favorable (*11*). The 140-keV gamma ray emitted by isomeric transition to ^{99m}Tc has almost ideal physical imaging characteristics (*12*). An infection imaging agent successfully labeled with ^{99m}Tc could be available widely at a small fraction of the cost required to produce most alternatives.

An injectable ^{99m}Tc-labeled IgM murine antibody to human stage specific embryonic antigen-1 (anti-SSEA-1) has been produced that recognizes several glycoproteins, including lacto-N-fucopentaeose-III (CD15), expressed on human white blood cells (WBCs) (*13,14*). As a result, systemically administered radioactivity becomes concentrated in areas of infection or inflammation where WBCs have already migrated (*15*). This obviates the need to withdraw any blood from a patient and significantly reduces the throughput time required to perform the test. Several preliminary trials have now demonstrated that, in the clinical setting, similar versions of this antibody preparation can effectively localize infections (*16–18*). In this study, biodistribution and radiation dosimetry of the antibody were evaluated systematically in healthy human volunteers without infections.

MATERIALS AND METHODS

The design of this study was similar to several others that we have reported previously (*19–23*).

Accrual and Assessment of Subjects

The subjects who participated in this study were recruited through advertisements in local papers and by word of mouth from other volunteers. Structured medical histories were taken, and physical examinations were performed. None of the volunteers had a known history of a health problem that could have affected significantly the biodistribution or elimination of radioligand at the

Received Apr. 8, 1998; revision accepted Aug. 4, 1998.
For correspondence or reprints contact: P. David Mozley, MD, 110-D Donner Building, HUP, 3400 Spruce St., Philadelphia, PA 19104.

time of study. None of the subjects was taking any medicines at the time of the study, except for oral contraceptives.

The final sample included 4 men and 6 women, whose diverse racial demographics tended to reflect those of the local population. They had a mean age ± SD of 30.2 ± 7.7 y (range 21–46 y). The 4 men had an average weight of 81.6 ± 14.8 kg and a mean height of 173.9 ± 4.8 cm (68.4 ± 1.9 in.). The 6 women weighed an average of 68.8 ± 17.0 kg, with a mean height of 171.8 ± 8.1 cm (67.6 ± 3.2 in.).

Radionuclide

Freshly eluted ^{99m}Tc pertechnetate (TcO_4) was obtained commercially from a ^{99m}Mo generator (Mallinckrodt Inc., St. Louis, MO).

Radiolabeling

The antibody was produced in vitro with cell hybridization techniques. Sterile and pyrogen-free lyophilized kits containing 250 μg of antiSSEA-1 were supplied by the study sponsor (LeuTech; Palatin Technologies, Inc., Princeton, NJ). The refrigerated kits were brought to ambient temperature before being reconstituted with 0.25 mL ^{99m}Tc generator eluate containing 20–40 mCi ^{99m}Tc. Each solution was incubated for 15 min at room temperature (≈20°C). At the termination of the incubation period, 0.75 mL ascorbic acid injection (Steris Laboratories, Inc., Phoenix, AZ), containing 250 mg/mL was added to the radiolabeled product as a diluent and stabilizer. Before administration, the final product was tested for the presence of free ^{99m}Tc pertechnetate by thin-layer chromatography (TLC) using 1.5 × 10 cm heat-treated instant TLC strips and methyl ethyl ketone as the mobile phase. Free ^{99m}Tc pertechnetate was below 1% in 9 subjects and below 3.8% in the other.

Measurements of Linear Attenuation

An uncollimated transmission source was prepared by dissolving about 1000 MBq ^{99m}Tc in a 1600-mL sheet flood made of Lucite. The rectangular dimensions of the sheet flood were about the same size as the collimators on a dual-head whole-body camera (Prism 2000; Picker International, Cleveland, OH). The flood was taped flat on top of the posterior projection collimator, which was always 40 cm from the surface of the anterior projection collimator on the upper head.

Nonattenuated scans of the transmission source were performed in the whole-body mode by acquiring images on the upper camera while the sheet source moved with it in tandem on the lower head. Scans were acquired for 10 min each over an excursion of 188 cm, which corresponded to 102 s/pixel.

The imaging table was then repositioned to a height designed to place the midcoronal plane of a typical adult in the center of the field between the two collimators. A whole-body transmission scan was then performed for 20 min (205 s/pixel). The other acquisition parameters were identical to the ones used to acquire the nonattenuated transmission images of the flood and the subsequent emission scans.

Emission Images

The radiopharmaceutical was injected as a bolus through an indwelling catheter in an antecubital vein. Dynamic images of the thorax and abdomen were acquired for 15 s per frame for 20 frames in a 256 × 256 matrix. The first whole-body scan was begun about 6 min after administration. Each whole-body scan was acquired in a 256 × 1024 matrix over a total excursion length of 188 cm. The pixel size was always 2.18 mm^2, which corresponded to scanning times of 102 or 205 s/pixel. The first 5 scans were acquired sequentially at 10 min per scan. The delayed images were acquired for 20 min at 2, 4, 6, 8, 22, 26 and 30 h postadministration.

Renal Excretion Fractions

Subjects were asked to micturate as often as possible during the first day of the study and to collect their urine overnight. The subjects produced an average of 11.4 ± 2.1 specimens over a mean of 27.9 ± 2.0 h (range 25.8–31.1 h). Images of the urine specimens were acquired with the same parameters used to scan the subjects, by laying the samples out flat on the imaging table. Corrections for attenuation were limited to accounting for absorption and scatter through the imaging table on which the specimens were placed. Attenuation by the urine itself was assumed to be negligible.

Image Analysis

The images were exported into a graphics workstation (Sun Microsystems, Mountain View, CA). An operator drew regions of interest (ROIs) around 17 different organs or tissues, the whole body, an off-body portion of the air and an off-body portion of the imaging table. The regions were drawn on whichever scan showed the organ most clearly after magnifying the images 2–16 times to facilitate tracing. Most organ boundaries were placed on the first whole-body scan, but the colon was always better visualized on the later images. The ROIs for the liver, spleen and kidneys were placed with a very high degree of confidence, because there was selective uptake and retention in these organs. The heart and lungs were clearly visualized on the first whole-body scan. The brain could be seen well as a photopenic region in the head, but the overlying skull and scalp could not be removed from its ROI. It was feasible to place testicular ROIs on the initial images of the men (n = 4). ROIs for the breasts in women (n = 6) were placed with less confidence on the transmission scans, because, with the exception of one young woman who was menstruating at the time of administration, there was no selective uptake in this sample to show true boundaries. The ROI for the nasal mucosa corresponded to a functional area of differentially increased uptake near the nose, which could be easily appreciated in most subjects. The thyroid gland could not be visualized in any of the volunteers. For this reason, the ROI representing the thyroid was large and stylized to reflect the nonspecific activity in the region of the thyroid fossa. Regardless of the scan from which it originated, each ROI was cut and pasted into a single master set. Once the set was complete, the ROIs were transposed onto all the other images, including the transmission scans through air and the subject. It was occasionally necessary for an operator to move the entire set of ROIs as a single unit to correct for repositioning errors between scans. It was also necessary to adjust the size of the ROIs for viscous organs, such as the urinary bladder, to account for normal changes in volume. In the case of the colon, each ROI had to be extensively revised from scan to scan. The last image that showed the colon best was used to estimate transmission. The ROI for the body almost always required minor revisions to correct for differences in pelvic tilt and position of the feet. Otherwise, individual ROIs were rarely manipulated independently of the other regions in the set. An automated subroutine measured the number of counts in these ROIs. Representative examples are shown in Figure 1.

Calculating the Activity in an Organ

Background corrections were performed by subtracting the product of the mean counts per pixel in the off-body ROI and the number of pixels in the ROI for an organ from the total number of counts in the ROI for that organ. The impact of this maneuver on

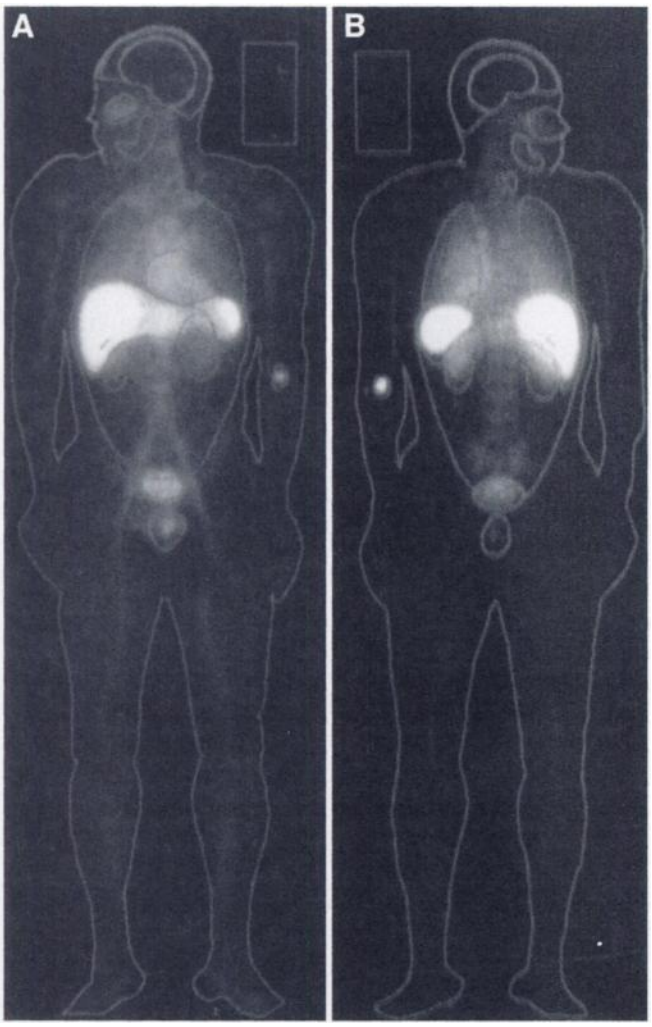

FIGURE 1. Representative emission images. (A) Early anterior image showing activity in vascular compartment. (B) Early posterior image.

the initial images was trivial (<1% in all cases). The low counting statistics and the large decay correction factors (>35) in the delayed images led to a mean reduction of about 7% at 30 h.

Attenuation corrections were applied from the experimentally measured ratio of counts in the transmission scans of the subjects on the imaging table and the forward-decay-corrected counts in the nonattenuated transmission scans through air.

Geometric means for each pair of decay, attenuation and background-corrected conjugate ROIs were calculated by multiplying the net anterior counts by the net posterior counts and taking the square root of the product. The fraction of the injected dose at each time point was then estimated by dividing the corrected geometric mean number of counts in each ROI or urine specimen by the net geometric mean number of counts in the initial whole-body image.

Checks were performed by adding the fraction of the dose in the ROI representing the whole body to the fraction of the dose excreted in the urine up until that time, and comparing the sum to the total number of counts in the first set of emission images.

Organ Residence Times

Mathematical simulations were used to generate time-activity curves for the bone marrow in the skull, the brain, breasts, heart, kidneys, liver, lungs, sacral bone marrow, spleen, thyroid and the urinary bladder. Multiexponential functions were fit iteratively to each time-activity curve using a nonlinear least squares regression algorithm. These curves were integrated numerically to yield source organ residence times.

Whole-body retention was estimated from the ROI encompassing the entire body minus the residual in the catheter hub. The remainder of the body residence time was calculated as the total body residence time minus the sum of all the other measured organ residence times, with the exception of those for the urinary bladder. In 7 of 10 subjects, this resulted in slightly negative numbers for the remainder of the body residence times at some time points. When this occurred, the remainder of the body residence times were assigned a value of zero.

The activity in the ROI encompassing the upper head minus the face was assumed to be in the bone marrow of the skull. It was also assumed that the activity in the marrow of the skull was representative of all other marrow spaces. The skull was assumed to contain 8.3% of the total active marrow (*24*).

The experimental measurements of activity voided in the urine were used to model the renal excretion rates. Parameters from the curve fits of the cumulative urinary excretion measurements were used as input data for the dynamic bladder model. However, residence times for the urinary bladder, and thus the dosimetry estimates that followed, were based on a theoretical bladder voiding interval of 4.8 h, or 5 times/d (*25*).

Activity not excreted in the urine was assumed to be eliminated in the feces. The colonic data were fit to the International Commission on Radiation Protection (ICRP) 30 gastrointestinal tract model to determine the small and large bowel residence times (*26*). The standard mass of tissue in each region of the gut was taken from ICRP 23 (*27*).

The residence times were used to estimate the absorbed doses with the MIRD technique using the MIRDOSE 3.1 software package (Oak Ridge Institute for Science and Education, Oak Ridge, TN) (*28*). For calculations in men, the masses of the organs and their spatial relationships with other bodily tissues were based on the (American) Adult Reference Man (*24,29*). The model assumed that the typical man was 170 cm tall and weighed 70 kg, whereas the actual values for this sample were 173.9 cm and 81.6 kg. Calculations for the female subjects were based on the Adult Reference Woman (160 cm and 58 kg), whereas the women in this sample were significantly taller and heavier (171.8 cm and 68.8 kg). The consequence was to overestimate the radiation absorbed doses, because both models assumed that the source organs were smaller and closer together than they actually were. The organ doses were calculated for each subject individually before results were averaged.

RESULTS

The initial images showed prolonged distribution in the vasculature with a mean half-time of elimination equal to 5.7 h in the blood. The great cerebral veins and the major blood vessels could be seen on the first whole-body scans. As time passed, the major vessels became progressively less well visualized. The bone marrow could be visualized throughout the axial skeleton for several hours after administration. The fraction of the administered dose in the bone marrow peaked on the first image. However, contrast between the concentration of radioactivity in bone marrow and background tissues

increased with time. Quantification showed that this was because radioactivity was eliminated from most tissues faster than from the bone marrow.

There was no uptake or retention by the salivary glands, even though they are known to contain SSEA-1. The gastric mucosa was never visualized. The thyroid could not be distinguished from the background in 8 subjects, and could be appreciated only on the initial images in the other 2.

Several tissues known to contain SSEA-1 were never visualized as regions of differentially increased uptake or retention, including the brain, breasts and eyes. No activity appeared to cross the blood-brain barrier. Low levels of persistent activity could be detected in the testes, but not the ovaries, although both contain SSEA-1.

Activity in the spleen initially increased with time until it peaked on the scans 25–35 min after administration. It then declined for the remainder of the study. Radioactivity was taken up by the liver rapidly. The fraction of the dose in the liver then increased continuously until it peaked about 1 h after administration, after which time the curves were essentially flat. An average of 40% of the injected dose could be recovered from the ROI for the liver for the remainder of the study. The curves for most of the other organs showed a peak on the first whole-body scan and then appeared to follow first-order kinetics. Activity could not be seen in the colon until 24 h postadministration.

Image analysis demonstrated that the administered radioactivity was excreted primarily by the renal system. Quantification showed that the renal excretion fractions varied from 31% to 49% over 26–31 h (mean ± SD = 39.5% ± 6.5%). Excretion was rapid and monophasic in 9 of the 10 volunteers, with an average biological removal half-time of 3.6 h (range 2.3–4.6 h). The renal excretion curve was biphasic in the other volunteer, with the majority of the activity (35.8%) excreted rapidly ($T_{1/2}$ = 3.5 h) and a smaller fraction (5.5%) excreted more slowly ($T_{1/2}$ = 26 h). This subject ingested relatively few fluids during the study, preferring to drink with his evening meal after leaving the laboratory. In 6 subjects, the estimated fecal excretion fractions over the course of the study ranged from 4% to 20%, with a mean of 10%. There was no fecal excretion during the study in the other 4 subjects. The total excretion (fecal and urinary) averaged 44% over 32 h (range 34%–57%).

The sum of the radioactivity excreted in the urine and the remaining radioactivity in the ROI for the whole body never varied by more than 3% of the injected dose during the first 8 h of study. It never varied by more than 5% during the first 24 h.

Calculations of the residence times in each organ (Table 1) showed that, on average, the largest value was in the whole body at 6.47 h (range 5.52–6.80 h), followed by that of the liver at 3.4 h (range 2.8–3.7 h).

Table 2 lists the absorbed dose estimates for the entire sample. The differences between men and women were minimal when compared to the variability within each group. The dose-limiting organ in both sexes was the spleen, which received an estimated 0.064 mGy/MBq (0.24 rad/mCi).

TABLE 1
Residence Times for ^{99m}Tc-Anti-SSEA-1

Source organ	Mean hours	Minimum hours	Maximum hours
Whole body	6.47	5.52	6.80
Liver	3.37	2.80	3.71
Marrow	1.09	0.76	1.60
Kidney	0.84	0.50	1.10
Spleen	0.65	0.18	0.88
Urinary bladder	0.59	0.42	0.70
Lung	0.43	0.32	0.63
Heart	0.21	0.14	0.29
Breast	0.19	0.07	0.32
Uterus	0.067	0.024	0.110
Brain	0.057	0.038	0.078
Remainder	0.041	0.000	0.195
Thyroid	0.016	0.012	0.020

DISCUSSION

The radiation dosimetry of the radiopharmaceutical seems favorable. If federal guidelines for research volunteers who

TABLE 2
Dose Estimates for ^{99m}Tc-Anti-SSEA-1

Organ	Mean mGy/MBq	Mean rad/mCi	Minimum rad/mCi	Maximum rad/mCi	SD %
Spleen	0.062	0.23	0.08	0.31	30
Kidneys	0.051	0.19	0.12	0.25	22
Liver	0.049	0.18	0.14	0.21	14
Bladder wall	0.032	0.12	0.08	0.16	24
Heart wall	0.017	0.062	0.046	0.083	20
Gallbladder wall	0.015	0.056	0.044	0.065	11
ULI wall	0.012	0.046	0.017	0.081	54
Pancreas	0.012	0.045	0.037	0.053	13
Adrenals	0.012	0.044	0.036	0.052	13
Lungs	0.012	0.044	0.032	0.061	20
Thyroid	0.011	0.042	0.033	0.054	20
Red marrow	0.010	0.038	0.029	0.052	17
Bone surfaces	0.0084	0.031	0.024	0.040	15
Small intestine	0.0081	0.030	0.014	0.049	43
LLI wall	0.0081	0.030	0.009	0.056	55
Breasts	0.0070	0.026	0.006	0.058	70
Stomach	0.0065	0.024	0.019	0.028	13
Uterus	0.0054	0.020	0.015	0.028	18
Total body	0.0051	0.019	0.015	0.022	13
Ovaries	0.0049	0.018	0.010	0.028	30
Muscle	0.0030	0.011	0.009	0.012	14
Thymus	0.0027	0.010	0.007	0.013	16
Brain*	0.0014	0.005	0.003	0.008	25
Skin	0.0014	0.005	0.004	0.005	14
Testes	0.0011	0.004	0.003	0.004	12
EDE†	0.018	0.068	0.054	0.085	16
Effective dose†	0.013	0.048	0.038	0.056	15

*Nonspecific radioactivity in the whole brain.

†Units of mSv/MBq and rem/mCi.

ULI = upper large intestine; LLI = lower large intestine; EDE = effective dose equivalent.

will not benefit from being exposed to ionizing radiation (*30,31*) were imposed clinically on patients being evaluated for infections, then 800 MBq (21.7 mCi) would still be an acceptable dose. This would expose the spleen to only 5 rads, less than a quarter of the radiation dose from 0.5 mCi ^{111}In-labeled WBCs and less than half the dose from 5 mCi ^{67}Ga citrate (*10*).

The estimate for the spleen as the radiation dose-limiting organ agrees well with the value previously reported in a dosimetry study of patients with infections (*18*). Estimates for the other eight organs listed in that report were generally two to three times lower than the values in this study. The systematic discrepancy may partially reflect biological differences between the healthy population represented in this study and patients with active infections, or the fact that the cohort in that report was older than the young adults in this study. It may also be possible that the lack of attenuation correction in the study of patients with infections produced artifactually low dose estimates for several solid organs.

Regardless, it is also possible that some of the conservative assumptions made in this study of healthy people artifactually inflated the dose estimates and contributed to systematic discrepancies with the earlier report. Use of the Standard Adult Female Phantom led to an overestimation of the radiation absorbed doses for women, because the volunteers in this study were significantly taller and heavier than the model assumed. As a result, the model assumed that the concentrations of activity in the source organs were higher and closer to one another than they actually were. In fact, the highest dose estimate to the spleen, the dose-limiting organ, was generated in the tallest woman in the sample.

Estimates to several other organs may be even more conservative. The calculated values for the urinary bladder were based on a theoretical voiding interval of 4.8 h, or five times per day. This assumption is standard in the dosimetry literature and was retained in this study to facilitate comparisons with other radiotracers. The estimated doses to the thyroid are even more conservative. The gland was only visualized in 2 subjects, and then only poorly on the early images. The ROIs for the thyroid were large and stylized, and probably reflected radioactivity in the vascular compartment of the thyroid and its surrounding fossa. The lack of any uptake in the salivary glands and gastric mucosa suggests that any contribution from free pertechnetate in the thyroid cells themselves was very small and is consistent with quality control procedures, which always showed that more than 96% of the injected dose was bound to the parent compound (>99% in 9 of 10 volunteers). Although the radioactivity was probably not in the thyroid cells of clinical concern, the modeling treated the radioactivity in the thyroid ROI as if it were.

Some uncertainty surrounds the dose estimates to the bone marrow. Attenuation within an organ ROI was most variable for this region, because of substantial differences between the flat bones imaged roughly *en face* to the collimator in their thickest projection and the flat bones imaged roughly perpendicular to the collimator in their thinnest projection. Early images of bone marrow activity indicated that the time-activity curves in the skull reflected the behavior of the tracer in other marrow spaces. However, activity excreted in the bowel prevented the sacrum from being used to corroborate findings on the later images. The initial images of activity in the vertebrae could not be interpreted because of blood-pool activity in the great vessels. This left the skull as the best representative of the bone marrow, despite estimates that included radioactivity in the overlying scalp and activity in the cerebral blood. As a result, estimates based on the experimental data are probably higher than some models would have predicted but lower than they would have been if any other bone marrow region had been used.

The lack of any uptake in the salivary glands and the gastric mucosa suggests that free ^{99m}Tc pertechnetate did not contribute significantly to the dosimetry. The dose estimates in these tissues were based on the experimental data, because they are known to contain the SSEA-1 antigen and would not have been modeled well without accounting for the potential of specific binding. However, the final analyses suggest that the impact of specific binding in these tissues was negligible, making it unclear whether this large, IgM antibody can access antigens in these regions.

CONCLUSION

The results indicate that the radiation dosimetry profile for this ^{99m}Tc-labeled IgM antibody to CD15 antigens on human granulocytes is highly favorable. The capacity of the methodology to conserve radioactivity over five physical half-lives and the relatively low intersubject variability tend to validate this technique for estimating absorbed radiation doses.

ACKNOWLEDGMENTS

This study was supported by a contract from Palatin Technologies, Inc., of Princeton, NJ, with supervision by Certus Intl., of St. Louis, MO.

REFERENCES

1. Raviglione MC, Snider DE Jr, Kochi A. Global epidemiology of tuberculosis. Morbidity and mortality of a worldwide epidemic. *JAMA*. 1995;273:220–226.
2. Datz FL. Abdominal abscess detection: gallium, ^{111}In- and ^{99m}Tc-labeled leukocytes, and polyclonal and monoclonal antibodies. *Semin Nucl Med*. 1996;26:51–64.
3. Lavender JP, Lowe J, Baker JR, Chaudri MA. Gallium-67 citrate scanning in neoplastic and inflammatory lesions. *Br J Radiol*. 1971;44:361–366.
4. Burleson RL, Johnson MC, Head H. Scintigraphic demonstration of experimental abscesses with intravenous ^{67}Ga citrate and ^{67}Ga-labeled blood leukocytes. *Ann Surg*. 1973;178:446.
5. McAfee JG, Thakur ML. Survey of radioactive agents for in vitro labeling of phagocytic leukocytes. I. Soluble agents. *J Nucl Med*. 1976;17:480–487.
6. McAfee JG, Thakur ML. Survey of radioactive agents for in vitro labeling of phagocytic leukocytes. II. Particles. *J Nucl Med*. 1976;17:488–494.
7. Shnier D, Bènard F, Alavi A, Garino J, Rhoad R. The promising role of FDG-PET imaging in suspected infection of orthopedic prostheses [abstract]. *J Nucl Med*. 1997;38:120P.
8. Shnier D, Bènard F, Alavi A, Garino J, Rhoad R. The role of FDG-PET in the diagnosis of osteomyelitis [abstract]. *J Nucl Med*. 1997;38:119P.

9. van der Laken CJ, Boerman OC, Oyen WJG, van de Ven MTP, van der Meer JWM, Corstens FHM. Scintigraphic detection of infection and inflammation: new developments with special emphasis on receptor interaction. *Eur J Nucl Med.* 1998;25:535–546.
10. Stabin MG, Stubbs JB, Toohey RE. *Radiation Dose Estimates for Radiopharmaceuticals.* Oak Ridge, TN: NUREG/CR-6345; 1996.
11. Steigman J, Eckelman WC. *The Chemistry of Technetium in Medicine.* Washington, DC: National Academy; 1992.
12. Sorenson JA, Phelps ME. *Physics in Nuclear Medicine.* 2nd ed. Philadelphia, PA: WB Saunders Co.; 1987.
13. Solter D, Knowles BV. Monoclonal antibodies defining a stage-specific mouse in ionic antigen (SSEA-1). *Proc Natl Acad Sci USA.* 1978;75:5565–5569.
14. Macher BA, Beckstead JH. Distribution of VIM-2 and SSEA-1 glycoconjugate epitopes among human leukocytes and leukemia cells. *Leukemia Res.* 1990;14:119–130.
15. Thakur ML, Richard MD, White FW III. Monoclonal antibodies as agents for selective radiolabeling of human neutrophils. *J Nucl Med.* 1988;29:1817–1825.
16. Thakur ML, Marcus CS, Henneman P, et al. Imaging inflammatory diseases with neutrophil-specific technetium-99m-labeled monoclonal antibody anti-SSEA-1. *J Nucl Med.* 1996;37:1789–1795.
17. Ahdoot R, Marcus CS, Thakur ML, et al. Rapid infection/inflammation imaging with Tc-99m-anti-SSEA-1 [abstract]. *J Nucl Med.* 1997;38:25P.
18. Gratz S, Behr T, Hermann A, et al. Intra individual comparison of a ^{99m}Tc-labeled anti-SSEA-1 antigranulocyte antibody and ^{99m}Tc-white blood cells for imaging infection. *Eur J Nucl Med.* 1998;25:386–393.
19. Mozley PD, Zhu XW, Kung HF, et al. The dosimetry of 3-Iodo-Schering 23390: Quantification of the radiation burden to healthy humans. *J Nucl Med.* 1993;34: 208–213.
20. Mozley PD, Stubbs JS, Kung HF, Selickson MH, Stabin MG, Alavi A. Biodistribution and dosimetry of I-123 IBF: A potent radioligand for imaging the D2 dopamine receptor. *J Nucl Med.* 1993;34:1910–1917.
21. Mozley PD, Stubbs JB, Kim H-J, et al. Dosimetry of a D2/D3 dopamine receptor antagonist that can be used with PET or SPECT. *J Nucl Med.* 1995;35:1322–1331.
22. Mozley PD, Stubbs JB, Kim H-J, et al. Dosimetry of an iodine-123-labeled tropane to image dopamine transporters. *J Nucl Med.* 1996;37:151–159.
23. Mozley PD, Stubbs JB, Plössl K, et al. The biodistribution and dosimetry of a ^{99m}Tc-labeled tropane for imaging dopamine transporters. *J Nucl Med.* 1998;39: 2069–2076.
24. Cristy M, Eckerman K. *Specific Absorbed Fractions of Energy at Various Ages from Internal Photon Sources.* ORNL/TM-8381. Oak Ridge, TN: Oak Ridge National Laboratory; 1987.
25. Cloutier RJ, Smith SA, Watson EE, Snyder WS, Warner GG. Dose to the fetus from radionuclides in the bladder. *Health Physics.* 1973;25:147–161.
26. International Commission on Radiation Protection. *Limits for Intake of Radionuclides by Workers.* ICRP Publication 30. New York, NY: Pergamon Press; 1979.
27. International Commission on Radiation Protection. *Report of the Task Group on Reference Man.* ICRP Publication 23. Oxford, UK: Pergamon Press; 1979.
28. Loevinger R, Berman M. *A Revised Schema for Calculating the Absorbed Dose from Biologically Distributed Radionuclides.* MIRD Pamphlet No. 1. Revised. New York, NY: Society of Nuclear Medicine; 1975.
29. Snyder WS, Ford MR, Warner GG, Watson SB. *"S" Absorbed Dose Per Unit Cumulated Activity for Selected Radionuclides and Organs.* MIRD Pamphlet No. 11. New York, NY: Society of Nuclear Medicine; 1975.
30. National Council of Radiation Protection and Measurements. *Basic Radiation Protection Criteria.* NCRP Report No. 39. Washington, DC: National Council of Radiation Protection and Measurements; 1971.
31. Food and Drug Administration, HHS. Radioactive Drugs for Certain Research Uses. *Code of Federal Regulations* (CFR) 21, Ch. 1 (4–1–89 Edition), Part 361.1, paragraph (b) (3) (i):206.